Seasonal budgets of reactive nitrogen species and ozone over the United States, and export fluxes to the global atmosphere

JOURNAL OF GEOPHYSICAL RESEARCH, VOL. 103, NO. D11, PAGES 13,435–13,450, JUNE 20, 1998

Seasonal budgets of reactive nitrogen species and ozone over the United States, and export fluxes to the global atmosphere

Jinyou Liang,[1] Larry W. Horowitz,[2] Daniel J. Jacob, Yuhang Wang,[3] Arlene M. Fiore, Jennifer A. Logan, Geraldine M. Gardner, and J. William Munger

Department of Earth and Planetary Sciences and Division of Engineering and Applied Sciences Harvard University Cambridge, MA

Abstract. A three-dimensional, continental-scale photochemical model is used to investigate seasonal budgets of O_3 and NO_y species (including NO_x and its oxidation products) in the boundary layer over the United States and to estimate the export of these species from the U.S. boundary layer to the global atmosphere. Model results are evaluated with year-round observations for O_3, CO, and NO_y species at nonurban sites. A seasonal transition from NO_x to hydrocarbon-limited conditions for O_3 production over the eastern United States is found to take place in the fall, with the reverse transition taking place in the spring. The mean NO_x/NO_y molar ratio in the U.S. boundary layer in the model ranges from 0.2 in summer to 0.6 in winter, in accord with observations, and reflecting largely the seasonal variation in the chemical lifetime of NO_x. Formation of hydroxy organic nitrates during oxidation of isoprene, followed by decomposition of these nitrates to HNO_3, is estimated to account for 30% of the chemical sink of NO_x in the U.S. boundary layer in summer. Model results indicate that peroxyacylnitrates (PANs) are most abundant in the U.S. boundary layer in spring (25% of total NO_y), reflecting a combination of active photochemistry and low temperatures. About 20% of the NO_x emitted from fossil fuel combustion in the United States in the model is exported out of the U.S. boundary layer as NO_x or PANs (15% in summer, 25% in winter). This export responds less than proportionally to changes in NO_x emissions in summer, but more than proportionally in winter. The annual mean export of NO_x and PANs from the U.S. boundary layer is estimated to be 1.4 Tg N yr^{-1}, representing an important source of NO_x on the scale of the northern hemisphere troposphere. The eventual O_3 production in the global troposphere due to the exported NO_x and PANs is estimated to be twice as large, on an annual basis, as the direct export of O_3 pollution from the U.S. boundary layer. Fossil fuel combustion in the United States is estimated to account for about 10% of the total source of O_3 in the northern hemisphere troposphere on an annual basis.

1. Introduction

Fossil fuel combustion accounts for about 50% of the total emission of nitrogen oxides (NO_x = NO + NO_2) to the atmosphere [*Intergovernmental Panel on Climate Change, (IPCC)*, 1995]. This anthropogenic source could have a major influence on the global budget of tropospheric O_3, considering that O_3 production in the troposphere is limited primarily by the supply of NO_x [*Chameides et al.*, 1992]. A moderating factor is the nonlinear dependence of O_3 production on NO_x. The number of O_3 molecules produced per molecule of NO_x oxidized to HNO_3 (O_3 production efficiency) decreases rapidly as the NO_x concentration increases [*Liu et al.*, 1987]. Most of the NO_x emitted by fossil fuel combustion is oxidized within the boundary layer of industrial continents, where NO_x concentrations are high and hence the O_3 production efficiency is low. An important factor determining the global influence of fossil fuel combustion on O_3 is the amount of NO_x exported out of the continental boundary layer and hence available to produce O_3 with high efficiency in the remote atmosphere [*Jacob et al.*, 1993a, b]. The export of NO_x may be facilitated by the formation within the continental boundary layer of peroxyacetylnitrate (PAN) and other peroxyacylnitrates from the oxidation of nonmethane hydrocarbons (NMHCs). These organic nitrates can be exported out of the boundary layer and serve as reservoirs for NO_x in the remote troposphere [*Crutzen*, 1979; *Singh*, 1987], in contrast to HNO_3 which is mainly removed by deposition.

We examine here the seasonal budgets of O_3 and NO_y species (including NO_x and its oxidation products) in the boundary layer over the United States and assess the implications for the export of NO_y species and O_3 to the global atmosphere. The United States is responsible for ~30% of global NO_x emissions from fossil fuel combustion [*Benkovitz et al.*, 1996]. Our analysis is based on a three-dimensional, continental-scale photochemical model for North America. A companion study by *Horowitz et al.* [this issue] uses a similar model to investigate in detail how summertime NMHC chemistry, involving in particular

[1]Now at Department of Civil and Environmnetal Engineering, Stanford University, Stanford, California.

[2]Now at National Center for Atmospheric Research, Boulder, Colorado.

[3]Now at School of Earth and Atmospheric Sciences, Georgia Institute of Technology, Atlanta, Georgia.

Paper number 97JD03126.
0148-0227/98/97JD-03126$09.00

the biogenic hydrocarbon isoprene, affects the chemical cycling of NO_y and the resulting export out of the boundary layer.

Several previous papers have examined the export of NO_y from North America. *Logan* [1983] estimated that 40% of NO_x emitted from North America is exported as NO_y, based on a balance between NO_x emission inventories and measured or inferred NO_y deposition fluxes. Similar percentages were reported by *Galloway et al.* [1984] using a climatological analysis of winds across the east coast of the continent, and by *Kasibhatla et al.* [1993] using a global three-dimensional model for NO_y. These analyses could not resolve the speciation of the exported NO_y nor did they determine seasonal variations. From a tropospheric chemistry perspective it is crucial to distinguish between the export of (NO_x + organic nitrates), which contributes to O_3 production in the remote troposphere, and the export of HNO_3 which generally does not lead to regeneration of NO_x. *Jacob et al.* [1993b] estimated that 6% of NO_x emitted in the United States is exported as NO_x from the U.S. boundary layer in summer, but they did not account properly for the export of organic nitrates nor did they consider other seasons besides summer.

The model analysis presented in this paper accounts for the speciation of NO_y and investigates seasonal variations of the export. We describe the model in section 2 and evaluate it with observations in section 3. Seasonal variations in the chemical regime of the U.S. boundary layer are discussed in section 4, and budgets for NO_y species are constructed in section 5. The contribution of fossil fuel combustion in North America to global tropospheric O_3 is examined in section 6.

Table 1. Chemical Tracers in the Model

Tracer	Component(s)
O_x (odd oxygen)	$O_3 + NO_2 + 2\,NO_3 + 3\,N_2O_5 + HNO_4$
H_2O_2	hydrogen peroxide
NO_x	$NO + NO_2 + NO_3 + HNO_2 + HNO_4 + 2\,N_2O_5$
HNO_3	HNO_3 + aerosol + NO_3^-
PAN	peroxyacetyl nitrate
PMN	peroxymethacryloyl nitrate
PPN(lumped)	peroxyacyl nitrates from RCHO
ISN2 (lumped)	isoprene nitrates
R4N2 (lumped)	$C_{4,5}$ alkylnitrates
CO	carbon monoxide
C_3H_8	propane
ALK4 (lumped)	>C_3 alkanes
ALKE (lumped)	>C_2 alkenes, except isoprene
C_5H_8	isoprene
CH_2O	formaldehyde
CH_3CHO	acetaldehyde
RCHO (lumped)	>C_2 aldehydes except MACR
CH_3COCH_3	acetone
MEK (lumped)	>C_3 ketones produced from ALK4
MVK	methylvinylketone
MACR	methacrolein

The lumping of organic compounds is done on a per carbon basis. Uniform concentrations of 1.7 ppmv CH_4 and 1.2 ppbv C_2H_6 are assumed over the model domain.

2. Model Description

2.1. General

We use an improved version of the continental-scale photochemical model originally presented by *Jacob et al.* [1993a]. Our model solves the three-dimensional continuity equations for 21 chemical tracers (Table 1) over a domain including North America and large portions of the neighboring oceans (Figure 1). Winds, convective mass fluxes, and other meteorological fields are from a 1-year simulation with a general circulation model (GCM) developed at the Goddard Institute of Space Studies (GISS) [*Hansen et al.*, 1983] and are updated every 4 hours. The grid resolution is 4°x5° in the horizontal, with 9 layers in the vertical along a sigma coordinate, replicating the grid of the GISS GCM (Figure 1). A nested subgrid scheme [*Sillman et al.*, 1990a] is used to resolve nonlinear chemistry in pollution plumes from large cities and power plants. Transport of tracers is as described by *Prather et al.* [1987]. A previous simulation of ^{222}Rn over North America showed that the model represents the ventilation of the continental boundary layer to within the constraints offered by ^{222}Rn observations, except over the eastern United States in fall where boundary layer mixing is excessive due to insufficient precipitation [*Jacob and Prather*, 1990; *Jacob et al.*, 1997].

Boundary conditions for O_3 concentrations at the edges of the model domain are specified as a function of altitude, latitude, and season from a climatology of ozonesonde data (J. A. Logan, manuscript in preparation, 1997). Longitudinal gradients in the ozonesonde data are small outside of the boundary layer at middle and high latitudes. Boundary conditions for CO are from a global three-dimensional model study (J. A. Logan, personal communication, 1997). Boundary conditions for NO_x, HNO_3, propane, butane, acetone, and H_2O_2 are specified as a function of altitude and latitude using aircraft data from the Pacific Exploratory Mission-West Phase A (PEM-West A) (September-October 1991) and Pacific Exploratory Mission-West Phase B (PEM-West B) (February-March 1994) aircraft missions over the western Pacific [*Gregory and Scott*, 1995a, b]; the PEM-West A and B data are used as boundary conditions in June-November

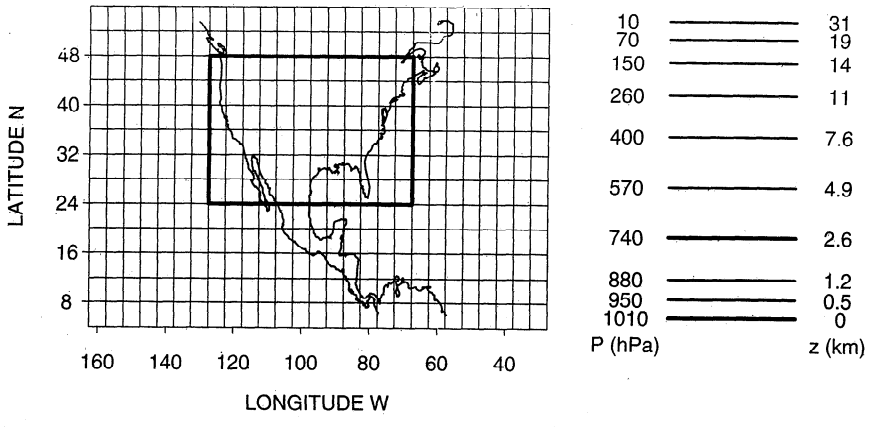

Figure 1. Model domain and grid. The edges of the figure are the boundaries of the model domain. The thick line delineates the U.S. boundary layer as defined in the paper for regional budget analyses.

and December-May, respectively. Boundary conditions for PAN during June-November are from PEM-West A. The PAN concentrations measured by *Singh et al.* [1997] at northern midlatitudes during PEM-West B range from about 500 parts per trillion by volume (pptv) in the lower troposphere to about 200 pptv at 500 hPa, considerably higher than the wintertime measurements of *Perros* [1994] over the western North Atlantic during the TROPOZ II aircraft mission which indicate a PAN concentration range of 50-100 pptv for the same latitudes. *Singh et al.* [1997] point out that the PEM-West B data for PAN could have been unusually affected by the outflow of continental pollution. As discussed in section 3, we can achieve in the model a good simulation of the *Perros* [1994] data and also of the wintertime data from a Canadian site by scaling down the model boundary condition for PAN during December-May by a factor of 10 from the PEM-West B data, essentially suppressing advection of PAN from outside the model domain; we choose to do so in the standard simulation. For all tracers other than those discussed above, we adopt low concentrations (1 pptv) as boundary conditions.

The simulations are conducted for 13 months, starting from the boundary conditions as initial conditions. The first month (May) is used for decay of the initial conditions (ventilation of the model domain requires less than 1 month). We focus our analysis on the last 12 months of simulation.

2.2. Chemistry

Chemical changes in tracer concentrations are computed with a fast Gear solver [*Jacobson and Turco*, 1994] applied to a photochemical mechanism for O_3-NO_y-hydrocarbon chemistry including detailed oxidation schemes for C_{1-4} alkanes, propene, and isoprene. The mechanism draws on compilations by *DeMore et al.* [1994] for inorganic and methane chemistry and by *Atkinson et al.* [1992] and *Atkinson* [1994] for NMHC chemistry; thermal decomposition rates for PAN and PPN are from *Grosjean et al.* [1994], and the chemistry of organic peroxy radicals (RO_2) includes new data from *Kirchner and Stockwell* [1996] and *Maricq and Szente* [1996a, b]. A discussion of the NMHC chemistry and a full listing of the isoprene oxidation mechanism are presented by *Horowitz et al.* [this issue]. Aqueous phase radical chemistry in clouds is ignored as it appears to have negligible effect on O_3 [*Liang and Jacob*, 1997]. Reactions in aerosols are calculated as a first-order loss defined by a reaction probability on the aerosol surface [*Dentener and Crutzen*, 1993]. We adopt a reaction probability of 0.1 for the hydrolysis of N_2O_5 to HNO_3 [*Mozurkewich and Calvert*, 1988] and for the conversion to HNO_3 of hydroxy organic nitrates produced by oxidation of alkenes and isoprene [*Shepson et al.*, 1996; P. B. Shepson, personal communication, 1996]. We also adopt a reaction probability of 0.1 for scavenging of HO_2 and hydroxy RO_2 radicals by aerosols. The spatial and temporal distribution of aerosols is based on a sulfate mass simulation by *Chin et al.* [1996] using the same GISS GCM meteorological fields. We compute the aerosol surface area from the sulfate mass in each gridbox by assuming that the aerosol particles are aqueous solutions of NH_4HSO_4 with a dry radius of 0.1 μm and liquid H_2O determined from thermodynamic equilibrium (Raoult's law) at the local relative humidity.

Actinic fluxes are computed hourly on the basis of the solar zenith angle, the GCM cloud optical depths (updated every 4 hours), and the total O_3 columns specified as a function of latitude and month [*Spivakovsky et al.*, 1990]. The radiation code uses a 6-stream approximation for the Rayleigh scattering atmosphere [*Logan et al.*, 1981]. Clouds are treated as reflective surfaces with reflectivities specified at four different altitudes to match the GCM vertical distribution of cloud optical depths [*Spivakovsky et al.*, 1990]. A light-absorbing aerosol is included with an optical depth of 0.1 at 310 nm varying inversely with wavelength.

The chemical mechanism used in this study is identical to that of *Horowitz et al.* [this issue] except for the aerosol uptake of HO_2, hydroxy RO_2 radicals, and hydroxy organic nitrates. *Horowitz et al.* [this issue] assumed reaction probabilities in aerosols of unity for HO_2 and zero for hydroxy RO_2 radicals and hydroxy organic nitrates; whereas we assume 0.1 for all these species. Because of the added aerosol sink for hydroxy RO_2 radicals and hydroxy organic nitrates in our model, concentrations in surface air over the eastern United States in summer are 5-10 parts per billion by volume (ppbv) lower than obtained by *Horowitz et al.* [this issue].

2.3. Emissions and Deposition

Anthropogenic emissions of NO_x, CO, and NMHCs from North America are based on 1990 national inventories for the United States [*U.S. Environmental Protection Agency (EPA)*, 1995] and Canada [*Environment Canada*, 1995], with spatial distributions from the National Acid Precipitation Assessment Program (NAPAP) [*U.S. EPA*, 1989]. Alkanes with ≥4 C atoms are emitted as ALK4 (Table 1) on a per-carbon basis, and alkenes with ≥3 C atoms are similarly emitted as ALKE on a per-carbon basis. Seasonal variations of NO_x and CO emissions are less than 10% [*U.S. NAPAP*, 1991] and are neglected. A 10% seasonal amplitude is applied to emissions of anthropogenic NMHCs, with maximum in summer and minimum in winter [*U.S. NAPAP*, 1991]. Anthropogenic emissions from Central and South America are as given by *Jacob et al.* [1993a] and do not vary with time of year.

Biogenic emission of isoprene is calculated hourly using the emission algorithm of *Guenther et al.* [1995] as modified by (Y. Wang et al., Global simulation of tropospheric O_3-NO_x-hydrocarbon chemistry, 1, Model formulation, submitted to *Journal of Geophysical Research*, 1997a) (hereinafter referred to as Wang et al., submitted manuscript, 1997a) and applied to the surface-type map of *Olson* [1992] with 0.5°x0.5° resolution. The emission varies with local temperature and light intensity and with the local leaf area index (LAI) which is updated monthly based on satellite observations of the global vegetation index (GVI). Seasonal observations of isoprene emission from forests in Colorado and Massachusetts indicate a time lag between the onset of photosynthesis and isoprene emission, with isoprene emission starting in early June and shutting off in late September [*Monson et al.*, 1995; *Goldstein et al.*, 1996]. In the model we restrict isoprene emission north of 40°N to the June-September time window. Biogenic emissions of other alkenes and acetone are scaled to that of isoprene with emission factors on a carbon basis of 0.051 for alkenes [*Goldstein et al.*, 1996] and 0.025 for acetone (Wang et al., submitted manuscript, 1997a).

Dry deposition fluxes of O_3, NO_x, peroxyacylnitrates, hydroxy organic nitrates, HNO_3, H_2O_2, and CH_2O are calculated locally using a big-leaf resistance-in-series model (Wang et al., submitted manuscript, 1997a) applied to the *Olson* [1992] surface-type map. The aerodynamic resistances are computed from archived GCM data for surface wind, solar irradiance at the surface, and nighttime cloud cover [*Jacob et al.*, 1993a]. The surface resistances vary with surface type, species type [*Wesely*, 1989], temperature, light intensity, monthly updated LAI, and snow cover in winter. Hydroxy organic nitrates are highly soluble in water [*Shepson et al.*, 1996] and are assumed to deposit like HNO_3. Wet deposition of highly water-soluble tracers (HNO_3, hydroxy organic nitrates, H_2O_2) is computed as described by *Balkanski et al.* [1993] from the GCM wet convective mass fluxes and synoptic precipitation fields; 100% scavenging of these tracers in precipitating convective updrafts is assumed.

3. Evaluation with Observations

The model is intended to simulate a typical meteorological year, rather than any given year; evaluation with observations must therefore focus on seasonal statistics. *Horowitz et al.* [this

Table 2. Observations Used for Model Evaluation

Species	Site	Length of Record
O_3 at surface	EPA/AIRS network	1980-1995[a]
	Harvard Forest, Massachusetts	1990-1994[b]
	Bermuda	Oct 1988-Sept 1991[c]
	Shenandoah Natl. Park, Virginia	Oct 1988-Oct 1989[d]
O_3 vertical profile	Boulder, Colorado	Dec 1984-Dec 1993[e]
	Wallops Island, Virginia	Jan 1980-Apr 1993[e]
NO_x	Harvard Forest, Massachusetts	1990-1994[b]
NO_y	Harvard Forest, Massachusetts	1990-1994[b]
	Shenandoah Natl. Park, Virginia	Oct 1988-Oct 1989[d]
PAN	Kejimkujik Natl. Park, Nova Scotia	Jun 1984-Apr 1989[f]
CO	Harvard Forest, Massachusetts	1990-1995[b]
	Shenandoah Natl. Park, Virginia	Oct 1988-Oct 1989[d]
NO_y deposition flux	Harvard Forest, Massachusetts	1990-1994[b,g]

[a] Long-term observations at 223 nonurban sites in the United States reported by the Aeronometric Information Retrieval Service (AIRS) and analyzed by *Fiore et al.* [1997]. Nonurban sites are selected on the basis of local NO_x emission densities, as described by *Fiore et al.* [1997]. We compute seasonal mean 1300-1600 local time (LT) concentrations for each site and individual years; from there we derive mean concentrations for each 4°x5° model grid square (Figure 1) in individual years by averaging the means for all sites in the grid square. Mean concentrations in the 4°x5° grid square for the 1980-1995 period are then obtained by averaging the grid square means for the individual years, and standard deviations are computed from the interannual variability.

[b] Five-year continuous record of hourly observations at Harvard Forest, Massachusetts. The concentrations of O_3, NO_x and NO_y are as reported by Munger et al. (submitted manuscript, 1997), and those of CO are unpublished data from J.W. Munger. Mean concentrations at 12-16 LT are computed for each month of individual years, excluding fresh pollution plumes diagnosed by $NO_x/NO_y > 0.8$ mol/mol. Monthly means are then averaged over the 5 years of the record, and standard deviations are computed from the interannual variability.

[c] From *Oltmans and Levy* [1992]. Concentrations are 24-hour averages.

[d] From *Poulida et al.* [1991] and *Doddridge et al.* [1992]. The observations are at 1100 m altitude on a mountain ridge. We select observed concentrations at 0000-0400 LT for comparison with the model in order to minimize the effect of upslope winds in observations.

[e] Ozonesonde observations reported by J.A. Logan (manuscript in preparation, 1997). Monthly means and standard deviations are for all observations within that month for the given time period. Seasonal mean concentrations are calculated from the appropriate monthly means.

[f] From *Sirois and Bottenheim* [1995]. Concentrations are 24-hour averages.

[g] Including both wet deposition of NO_3^- and dry deposition of NO_y measured separately (Munger et al., submitted manuscript, 1997).

issue] presented a detailed evaluation of the model for summer. Surface air concentrations of O_3 over the south central United States in summer were overestimated by 10-30 ppbv, due to insufficient ventilation of the region in the GCM by maritime air from the Gulf of Mexico. The observed O_3 versus CO and O_3 versus (NO_y-NO_x) correlations and corresponding slopes were closely reproduced, implying a good simulation of the O_3 production efficiency. The model simulated to within about 30% the observed median summer concentrations of NO_x, PAN, HNO_3, and NO_y at nonurban sites in North America and captured to within 10% the observed speciation of NO_y among NO_x, PAN, and HNO_3 at individual sites.

We extend here the evaluation presented by *Horowitz et al.* [this issue] to investigate seasonal variations. For this purpose, we use time series of observations at non-urban sites that are at least 1 year long (Table 2). Unless otherwise indicated, we limit our comparison to early afternoon when surface air measurements are most likely to be representative of a deep mixed layer that can be resolved with the model. The concentration statistics sampled in the model exclude the pollution plumes resolved with the subgrid plumes scheme [*Sillman et al.*, 1990a] and are thus representative of rural conditions.

3.1. Ozone

Figure 2 compares the simulated and observed distributions of O_3 concentrations in surface air over the United States for different seasons. The observations are from the EPA Aeronometric Information Retrieval Service (AIRS), as described in Table 2. The highest observed concentrations are over the eastern United States and southern California in summer, and these are captured by the model to within 10 ppbv. The model overestimates O_3 by 10-20 ppbv in the south central United States in summer and fall, a discrepancy discussed by *Horowitz et al.* [this issue]. The regional depletion of O_3 over the northeastern United States in winter, found both in the model and in the observations, reflects destruction of O_3 by NO emissions; oxidation of NO to HNO_3 via hydrolysis of N_2O_5 in aerosols (the principal sink of NO_x in winter) consumes 1.5 molecules O_3 per molecule of NO oxidized.

To assess the ability of the model to reproduce the spatial variance of O_3 concentrations over the United States, we show in Figure 3 a statistical summary of simulated versus observed concentrations in 4°x5° grid squares for the data in Figure 2. The least squares correlation coefficient r^2 between model and observations ranges from 0.55 to 0.65 depending on season. The model has a mean bias of -2 to +3.5 ppbv.

Simulated and observed seasonal variations of O_3 concentrations are compared in Figure 4. The model captures the spring-summer maximum over the United States, although the seasonal peak in the model over the eastern United States is shifted to the end of the summer (August) reflecting the seasonal peak in GCM temperatures [*Jacob et al.*, 1993a]. The amplitude of the seasonal cycle is larger in the eastern than in the western United States, both in the observations [*Logan*, 1989] and in the model; this regional difference is driven by the high NO_x emissions in the east, which promote O_3 formation in summer but act to deplete O_3 in winter. Also shown in Figure 4 is a comparison of model results to observations for Bermuda [*Oltmans and Levy*, 1992]. The model reproduces well the observed seasonal cycle characterized by a spring maximum and summer minimum.

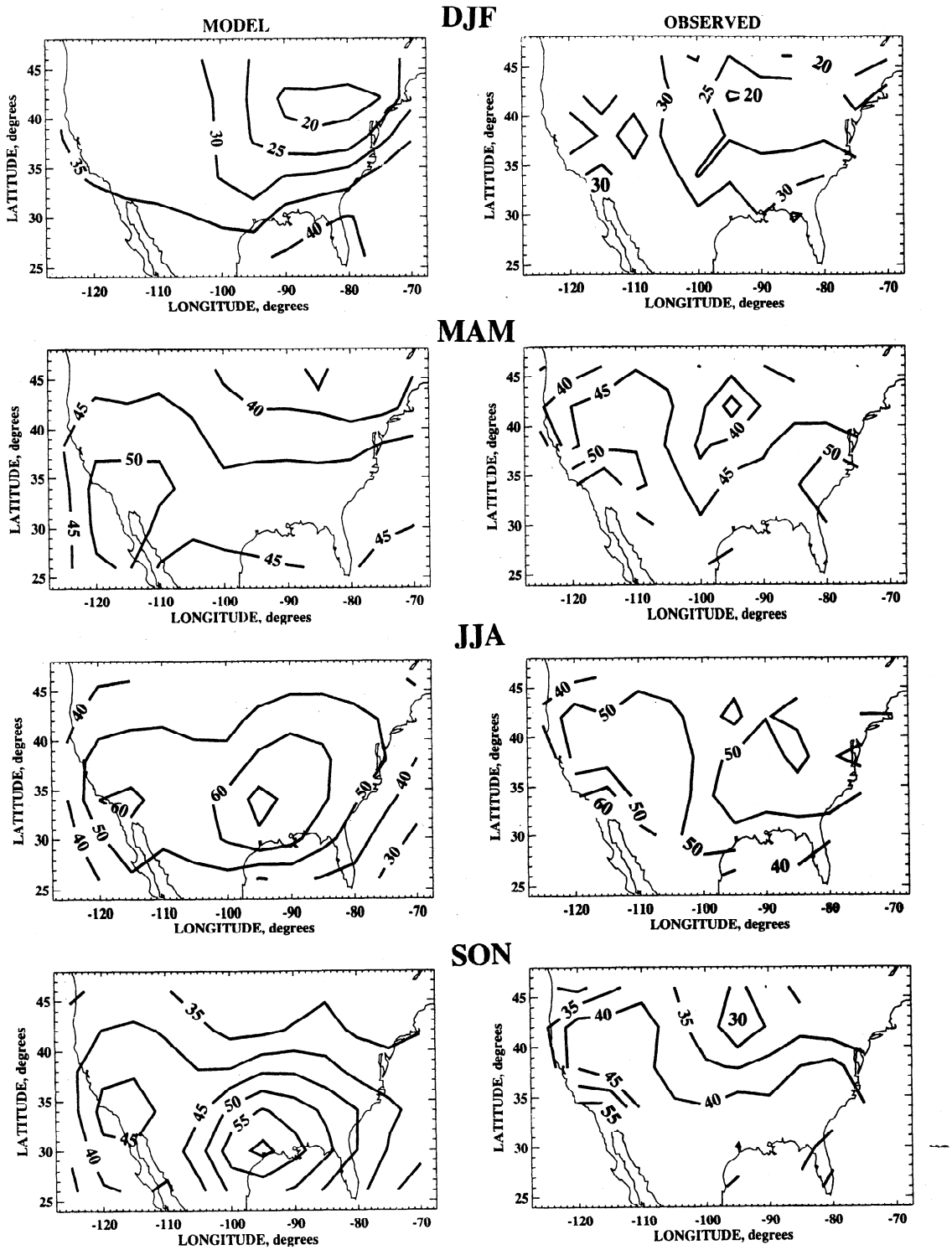

Figure 2. Mean afternoon (1300-1600 local time) O_3 concentrations (ppbv) in surface air over the United States in different seasons. Model results (left panels) are compared to 1980-1995 observations from the EPA Aeronometric Information Retrieval Service (AIRS). Contours are at 5 ppbv intervals except for the summer panel where they are at 10 ppbv intervals.

Advection of boundary conditions, chemistry, and deposition all play a role in shaping the distribution of O_3 in the model. In order to isolate these influences we conducted two sensitivity simulations: (1) a "no-chemistry" simulation where O_3 is solely controlled by transport from the boundaries and deposition; (2) a "zero-NO_x" simulation where no NO_x is emitted from the model domain. In the latter simulation, advection of NO_x and PAN from the boundaries maintains a background NO_x concentration of 2-50 pptv in the boundary layer over the United States. Comparison of these sensitivity simulations to the standard simulation in Figure 4 shows that regional production makes an important contribution to O_3 concentrations in surface air over the United States in all seasons except winter. Ozone concentrations in the zero-NO_x simulation are 20-40 ppbv, with little seasonal varia-

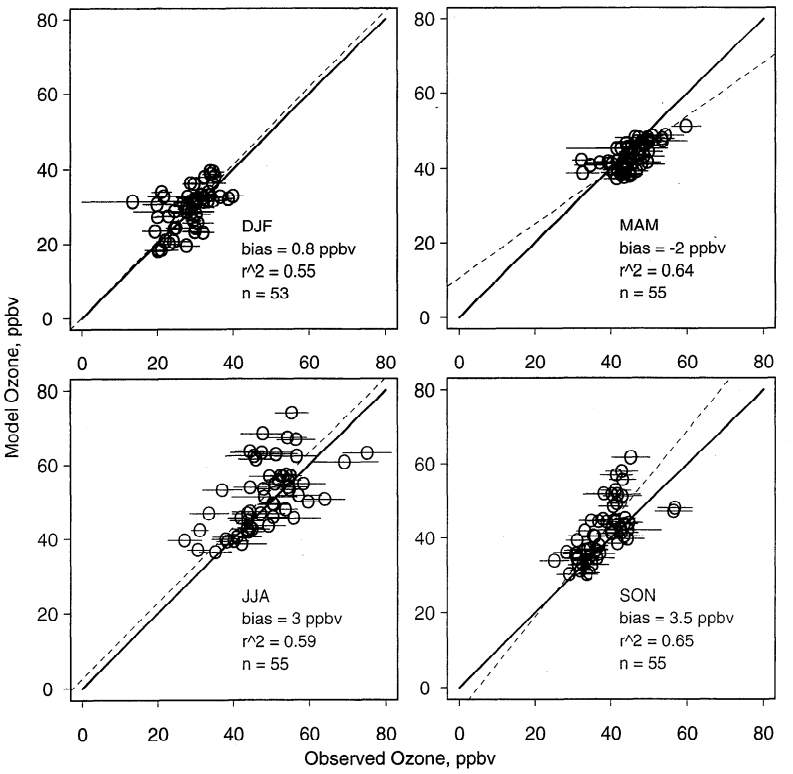

Figure 3. Scatterplots of simulated versus observed seasonal mean O_3 concentrations (ppbv) in surface air over the United States at 1300-1600 local time. Data are shown for all 4°x5° grid squares where EPA/AIRS data are available [*Fiore et al.*, 1997]. When several EPA/AIRS sites are present in one grid square, the data are first averaged over all sites for a given year and then over the 16-year record; the corresponding standard deviations (horizontal bars) are defined by the interannual variability of the seasonal mean concentrations for individual years. Also shown on the figure are the 1:1 line (solid lines), the least-squares regression line calculated with the reduced major axis method (dashed lines), the least squares correlation coefficient r^2, and the mean bias defined as $1/n \sum_n([O_3]_{model}-[O_3]_{obs})$ for all points on the plot.

tion. The summer minimum at Bermuda is caused by photochemical loss.

Simulated vertical profiles of O_3 concentrations in different seasons are compared in Figure 5 to the ozonesonde data from Wallops Island, Virginia and Boulder, Colorado. The model underestimates O_3 concentrations over Wallops Island by 10-20 ppbv in summer; other seasons are simulated better. Regional production of O_3 from NO_x emissions in the United States, as diagnosed by the difference between the standard and zero-NO_x simulations, accounts for more than 10 ppbv of O_3 up to 700 hPa altitude over Wallops Island in all seasons except winter. In winter, NO_x emissions cause a 5 ppbv depletion of simulated O_3 concentrations near the surface; surface depletion is also apparent in the observations. Over Boulder, simulated O_3 concentrations in winter are largely controlled by advection of boundary conditions, but in other seasons there is an important contribution from regional photochemical production extending up to 500 hPa.

3.2. NO_y Species and CO

Figure 6 compares simulated and observed seasonal variations of NO_x, NO_y, and CO concentrations at Harvard Forest, Massachusetts. Also shown is the NO_x/NO_y concentration ratio. The hourly observations used to construct the monthly means were filtered to remove fresh pollution plumes as diagnosed by NO_x/NO_y > 0.8 mol/mol (in the model, pollution plumes are effectively removed by the subgrid plumes scheme). Model and observations show summer minima and winter maxima for all species, due in part to seasonal variations in mixing depth [*Holzworth*, 1967], and also in the case of NO_x to the longer lifetime in winter (J. W. Munger et al., Regional budgets for nitrogen oxides from continental sources: Factors affecting oxidation and deposition, submitted to *Journal of Geophysical Research,* 1997) (hereinafter referred to as Mu;nger et al., submitted manuscript, 1997). The strong seasonal variation of the NO_x/NO_y concentration ratio is captured by the model and largely reflects the seasonal variation in the lifetime of NO_x (see discussion in section 5). The model underestimates NO_y concentrations in spring and fall, a problem which we attribute to precipitation anomalies over the eastern United States in the GCM [*Jacob and Prather*, 1990]. The GCM spring is wetter than normal, resulting in efficient scavenging of HNO_3 and thus relatively low NO_y concentrations but high NO_x/NO_y ratios (Figure 6). Conversely, the GCM fall is drier than normal, resulting in a deep boundary layer and low concentrations of both NO_y and CO (note that CO is underestimated in the fall but not in the spring).

Figure 7 compares simulated and observed seasonal variations of NO_y and CO concentrations at Shenandoah National Park, Virginia (1100 m altitude). Concentrations of NO_y show a summer minimum and winter maximum, both in the model and in observations, as at Harvard Forest. Spring and summer NO_y concentrations in the model are too low by a factor of 2. Observed concentrations of CO also show a summer minimum and winter maximum, except for high values in July-August which are neither captured by the model nor seen in the Harvard Forest observations. *Poulida et al.* [1991] attributed the high summer CO values in the observations to the effect of isoprene

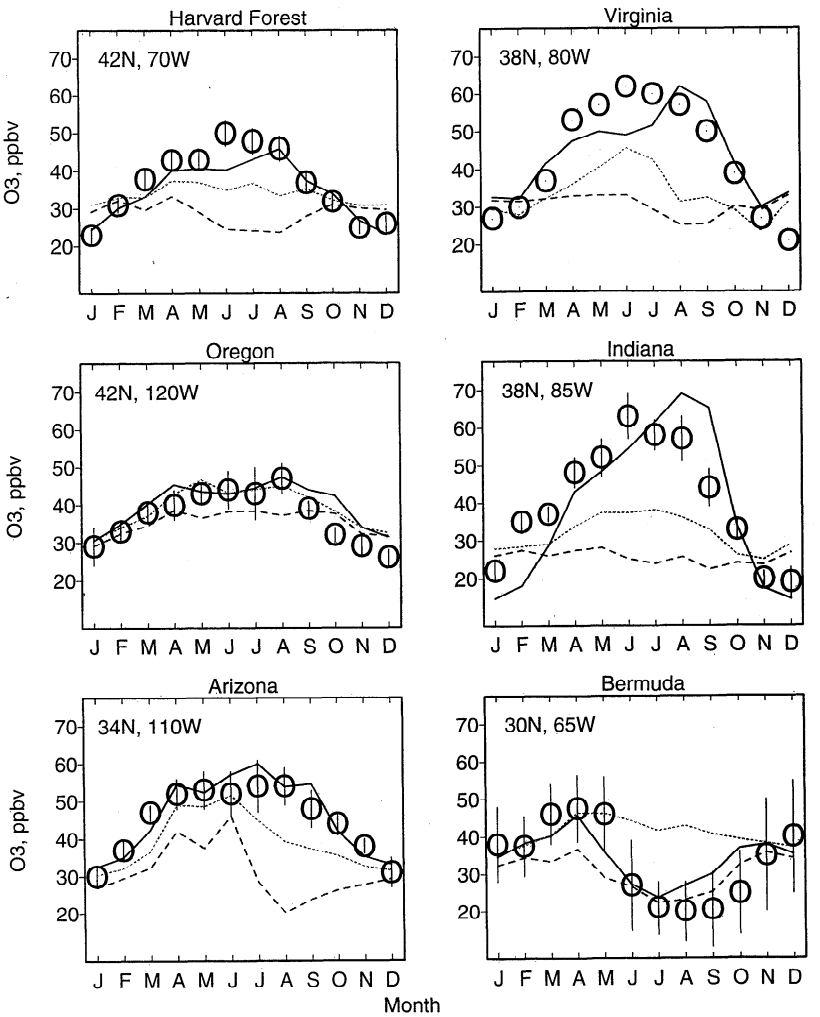

Figure 4. Seasonal variation of simulated and observed monthly mean O_3 concentrations (ppbv) in surface air at 1300-1600 local time. Observed monthly means for 1980-1995 are plotted as open circles; the vertical bars are the interannual standard deviations. Model results are shown for the standard simulation (solid lines), the no-chemistry simulation (dotted lines), and the zero-NO_x simulation (dashed lines). The observations are from the EPA/AIRS network averaged over 4°x5° grid squares (the center of the grid square is indicated), except for Harvard Forest (Munger et al., submitted manuscript, 1997) and Bermuda [*Oltmans and Levy*, 1992]. Concentrations at Bermuda are 24-hour averages.

oxidation, but the implied isoprene emission would be exceedingly high. We find in the model that isoprene oxidation contributes less than 30 ppbv CO at the site in summer (results from a simulation without isoprene emission are shown as dashed lines in Figure 7).

To our knowledge, the only year-round record for PAN concentrations in non-urban air in North America is from Kejimkujik National Park, Nova Scotia [*Sirois and Bottenheim*, 1995]. Comparison between model and observations is shown in Figure 8. The seasonal maximum is in February-March in the observations and March-May in the model; the model overestimates PAN concentrations in all seasons except winter. Day-to-day variability in the model is considerable, as shown by the dashed lines (standard deviations of daily concentrations). This variability reflects the contrast in influence at the site between air masses with elevated PAN advected from the eastern United States and air masses with low PAN advected from the north. *Horowitz et al.* [this issue] showed that the model reproduces to within 30% the observed PAN concentrations over the eastern United States in summer, with no evident bias. We explain the excessive PAN in the model at Kejimkujik as caused by too frequent transport of air from the eastern United States to the site in summer, a problem previously noted by *Chin et al.* [1996] in their simulation of summertime sulfate over eastern Canada using the same meteorological fields.

As discussed in section 2, the model boundary condition for PAN concentrations during December-May was scaled down by a factor of 10 from the PEM-West B observations. This allows model results to match roughly not only the wintertime PAN concentrations observed at Kejimkujik but also the TROPOZ-II aircraft observations of PAN by *Perros* [1994] over the western North Atlantic in January, which ranged from about 100 pptv in the lower troposphere to 50 pptv at 500 hPa. We find that use of the PAN concentrations from PEM-West B flights as a model boundary condition would lead to an overestimate of the wintertime Kejimkujik and TROPOZ-II data by factors of 2 to 4.

3.3 Nitrate Deposition

We compare in Figure 9 the simulated and observed seasonal variations of nitrate deposition fluxes (separately for wet and dry)

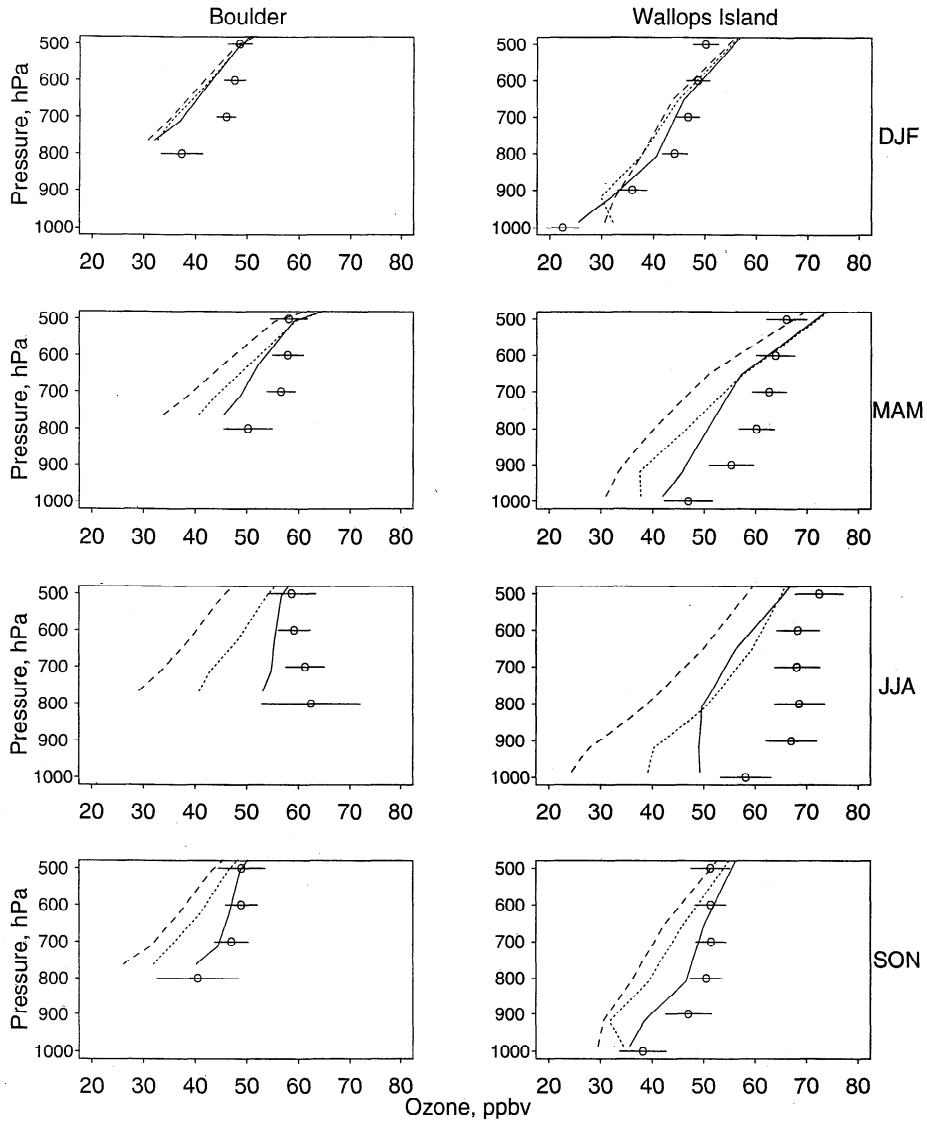

Figure 5. Seasonally averaged vertical profiles of O_3 concentrations over Boulder, Colorado (835 hPa surface) and Wallops Island, Virginia. Observations (Table 2) are plotted as open circles; horizontal bars represent the interannual standard deviations. Model results are shown for the standard simulation (solid lines), the no-chemistry simulation (dotted lines), and the zero-NO_x simulation (dashed lines).

at Harvard Forest. The observations show a weak winter minimum which Munger et al. (submitted manuscript, 1997) attributed to a lesser abundance of HNO_3, the main depositing form of NO_y, during that season. The model reproduces to within 20% the mean deposition fluxes of NO_y in individual seasons, except in the fall when the model is too low by almost a factor of 2. The fall anomaly is partly due to low GCM precipitation in the region, as discussed previously. The drought not only suppresses removal by wet deposition, but also increases boundary layer mixing and hence slows down dry deposition as well. We find that hydroxy organic nitrates formed from the oxidation of isoprene with a 12% yield [*Horowitz et al.*, this issue] contribute 23% of the total summertime deposition of nitrate at Harvard Forest in the model. These organic nitrates decompose rapidly to NO_3^- in aqueous solution (P. B. Shepson, personal communication, 1996) and hence would be measured as NO_3^- in precipitation samples.

4. Seasonal Variation in Photochemical Regime

Theoretical arguments and limited observations suggest that a seasonal transition from NO_x- to NMHC-limited conditions for O_3 production should take place over the eastern United States in September because of decreasing UV radiation and the end of isoprene emission [*Jacob et al.*, 1995]. We examined this issue in our three-dimensional model by conducting sensitivity studies with either NO_x or NMHC emissions reduced by a factor of 2 over the model domain (the reduction of NMHC emissions was applied to both anthropogenic and biogenic sources). Changes in the simulated seasonal mean O_3 concentrations are shown in Figure 10. In summer, O_3 production is strongly NO_x-limited, as noted in previous model studies [*Trainer et al.*, 1987; *Sillman et al.*, 1990b; *McKeen et al.*, 1991; *Jacob et al.*, 1993b]; halving NO_x emissions decreases O_3 concentrations by 10-20 ppbv over most of the United States, while halving NMHC emissions decreases O_3 concentrations by less than 5 ppbv. In winter, by

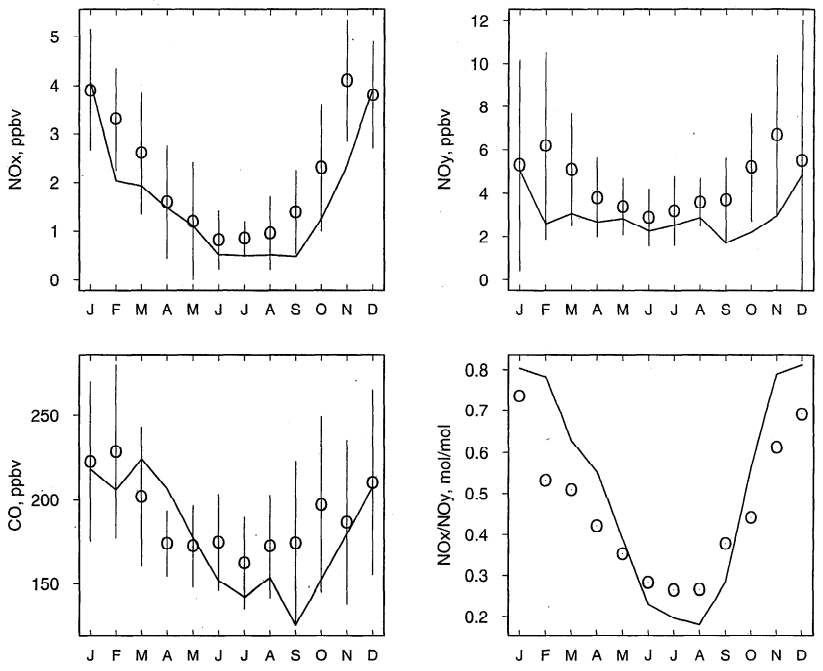

Figure 6. Seasonal variations of monthly mean concentrations of NO_x, NO_y, and CO and NO_x/NO_y concentration ratios at Harvard Forest, Massachusetts, at 1200-1600 local time. Observations for 1990-1994 (Table 2) are plotted as open circles; the vertical bars are the interannual standard deviations. Model results are plotted as solid lines.

contrast, halving NO_x emissions causes an increase in O_3 concentrations, particularly in the northeast, because conversion of NO_x to HNO_3 by hydrolysis of N_2O_5 represents a major sink for O_3 in that season. The largest sensitivity to NMHC emissions is in the fall (September-November) in the eastern United States, when photochemistry is still active but mostly NMHC-limited, as proposed by *Jacob et al.* [1995].

5. Seasonal Budget of NO_y Species

Table 3 summarizes the model budgets for the U.S. boundary layer of NO_y emitted by fossil fuel combustion within the region in different seasons. The U.S. boundary layer is defined as the region extending horizontally over the area delineated by thick lines in Figure 1 and vertically from the surface to the top of model layer 3 (about 740 hPa). The NO_y budget in the zero-NO_x simulation was subtracted from that in the standard simulation in order to remove the small influence of NO_y advected from outside the region; the correction is less than 20% for most terms in the Table.

We see from Table 3 that the NO_y pool is dominated by NO_x, HNO_3, and PAN in all seasons. Organic nitrates other than PAN contribute 10% of NO_y in summer and 5% in other seasons. The fraction of NO_y present as NO_x is maximum in winter (60%) and minimum in summer (20%), while that present as HNO_3 is minimum in winter (25%) and maximum in summer (55%). In spring and fall, NO_x and HNO_3 each account for 30-45% of NO_y. The contribution of PAN to NO_y is largest in spring (20%) and smallest in winter (6%). Although the lifetime of PAN is longest in winter because of the low temperatures, photochemical oxidation of NMHCs is then at its seasonal minimum and hence there is little production of PAN. The high PAN concentrations in spring reflect a combination of low temperatures and active photochemistry. Oxidation of isoprene provides the dominant source of PAN in summer [*Horowitz et al.*, this issue].

The mean seasonal variation of the NO_x/NO_y ratio in the U.S. boundary layer in the model is similar to that previously shown for Harvard Forest (Figure 6). Munger et al. (submitted manuscript, 1997) proposed that this seasonal variation is driven primarily by seasonal changes in the lifetime of NO_x, and we find in the model that this is indeed the case. The model lifetime of NO_x in the U.S. boundary layer ranges from 0.3 days in summer to 1.2 days in winter; the model lifetime of HNO_3 varies less, ranging from 0.5 day in spring to 1.1 days in fall (Table 3). As previously discussed, most of the seasonality in the HNO_3 lifetime in the model is driven by the spring maximum and fall minimum of precipitation over the eastern United States in the GCM year, whereas climatological data show little seasonal variation of precipitation in this region. During summer, formation of hydroxy organic nitrates by oxidation of isoprene followed by rapid decomposition of these organic nitrates to HNO_3 accounts for 30% of total HNO_3 formation and hence represents an important sink pathway for NO_x. In winter, production of HNO_3 is dominated by hydrolysis of N_2O_5 in aerosols, which is limited by the rate of NO_3 production from the NO_2+O_3 reaction.

On an annual basis, 30% of the NO_x emitted in the United States is exported out of the U.S. boundary layer as NO_y (25% in summer, 35% in winter). Our estimate of the annual mean export is consistent with previous studies [*Logan*, 1983; *Galloway et al.*, 1984; *Kasibhatla et al.*, 1993]. The seasonal variation in NO_y export reflects the seasonal variation of the HNO_3/NO_y concentration ratio in the U.S. boundary layer, as HNO_3 is the main depositing component of NO_y; a larger fraction of HNO_3 implies a shorter lifetime of NO_y against deposition and hence less NO_y export.

From a global tropospheric chemistry perspective, export of NO_y as HNO_3 is of limited interest because most of this HNO_3 will be removed eventually by deposition. The critical components of the exported NO_y are NO_x, which drives O_3 production in the remote troposphere, and peroxyacylnitrates (PANs), which eventually decompose to NO_x; we refer to the sum of these two NO_y components as "NO_x + PANs." We find in the model that most of the NO_y exported from the U.S. boundary layer is in the form of NO_x + PANs, 60-80% depending on season (Table

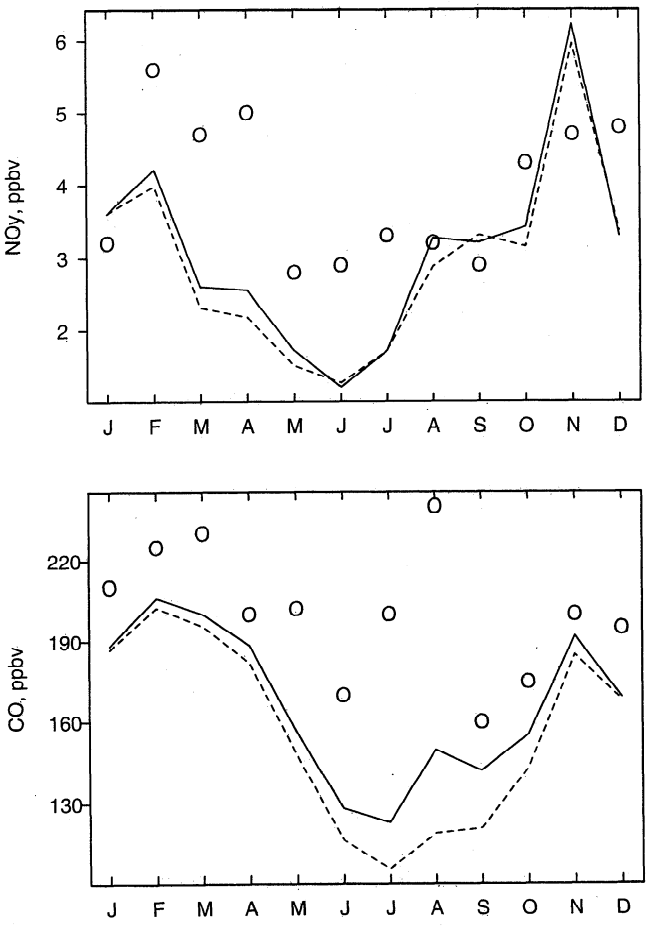

Figure 7. Seasonal variation of monthly mean concentrations of NO_y and CO at Shenandoah National Park, Virginia (mountain ridge site, 1100 m altitude). The observations were sampled at 0000-4000 LT to avoid the effect of daytime upslope flow [*Poulida et al.*, 1991] while model results are 24-hour averages sampled in model layer 2 (Figure 1). Observations (Table 2) are plotted as open circles, and model results are plotted as solid lines. The observations are for 1 year only, hence no interannual standard deviations are shown. The dashed lines show model results for a simulation without emission of isoprene.

3). Although NO_x + PANs account for only 40% of NO_y in the U.S. boundary layer in summer, export of NO_y in that season takes place principally by wet convection (Figure 11 [see also *Jacob et al.* 1993b; *Thompson et al.* 1994]) during which HNO_3 is efficiently scavenged. By contrast, in winter most of the export is by advection northward and eastward in the lower troposphere (Figure 11), and the speciation of NO_y in the exported air reflects more closely the speciation in the U.S. boundary layer. The NO_x/PANs concentration ratio in the exported air ranges from 1 in summer to 5 in winter, reflecting the partitioning in the boundary layer air (Table 3).

To investigate the response in the export of NO_x+PANs to changes in NO_x emissions, we conducted simulations where NO_x emissions in the U.S. boundary layer domain were increased or decreased by a factor of 2. Results are shown in Figure 12. In summer when photochemistry is NO_x-limited, increasing NO_x emission leads to an increase in OH concentrations and hence a decrease in the NO_x lifetime; the export of NO_x+PANs responds less than proportionally to the change in emission. By contrast, in winter when photochemistry is NMHC-limited, doubling NO_x emissions increases the lifetime of NO_x (because of lower O_3 concentrations, slowing down the rate of the $NO_2 + O_3$ reaction), and the export of NO_x+PANs responds more than proportionally.

6. Global Implications for Ozone

The yearly export of NO_x+PANs out of the U.S. boundary layer in the model is 1.4 Tg N yr^{-1} (0.27 Gmol d^{-1}), which can be compared to northern hemisphere estimates of NO_x sources from lightning (1.7 Tg N yr^{-1}) ([Wang et al., submitted manuscript, 1997a) and aircraft (0.4 Tg N yr^{-1}) [*Baughcum et al.*, 1996]. Export of pollution from the United States is clearly a major source of NO_x to the northern hemisphere troposphere, in all seasons.

To estimate the eventual source of O_3 from the exported NO_x + PANs, we calculated from our model the O_3 production efficiency (OPE) in the U.S. boundary layer and in the band of adjacent grid boxes (Figure 11). The OPE is defined as the gross number of odd oxygen (O_x) molecules produced from a NO_x molecule before it is oxidized to HNO_3, which is then assumed to be removed by deposition [*Liu et al.*, 1987]. We calculate the OPE for a region in the model as the ratio of O_x to HNO_3 production averaged over the region. The OPE ranges from 3 in winter to 16 in summer in the U.S. boundary layer and from 35 in winter to 61 in summer in the free troposphere (Figure 11). By applying the OPE for each region to the corresponding export fluxes of NO_x + PANs (Figure 11), we estimate a source of O_3 to the global troposphere ranging from 5 Gmol d^{-1} in winter to 11 Gmol d^{-1} in summer, for an annual average of 8.0 Gmol d^{-1}. A more accurate estimate would require a global simulation.

The above source of O_3 can be compared to the direct export of O_3 pollution from the United States. A model budget for O_3 (Table 4) shows that the U.S. boundary layer is a net sink for O_3 in winter and spring and a net source in summer and fall. This budget can be viewed as the difference between the import of background O_3 from outside the U.S. boundary layer and the export of pollution O_3 produced within the region. We obtain a budget for pollution O_3 in the model (Table 4) as the difference between results from the standard simulation and from the zero-NO_x simulation (where only the import of background O_3 is considered). The export of pollution O_3 from the U.S. boundary layer is thus defined analogously to that of fossil fuel NO_y discussed in the previous section. Of the 7.9 Gmol d^{-1} of pollution O_3 produced within the U.S. boundary layer on an annual mean basis, 35% is chemically consumed within the boundary layer (mostly by the $O^1D + H_2O$ reaction), 15% is deposited, and 50% is exported. Export of pollution O_3 from the U.S. boundary layer

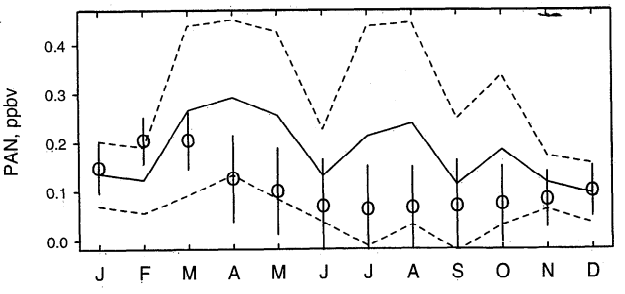

Figure 8. Seasonal variation of monthly mean concentrations of PAN at Kejimkujik National Park, Nova Scotia. Observations (Table 2) are shown as open circles, with interannual standard deviations as vertical lines. Model results are shown as solid lines, with standard deviations of daily concentrations shown as dashed lines.

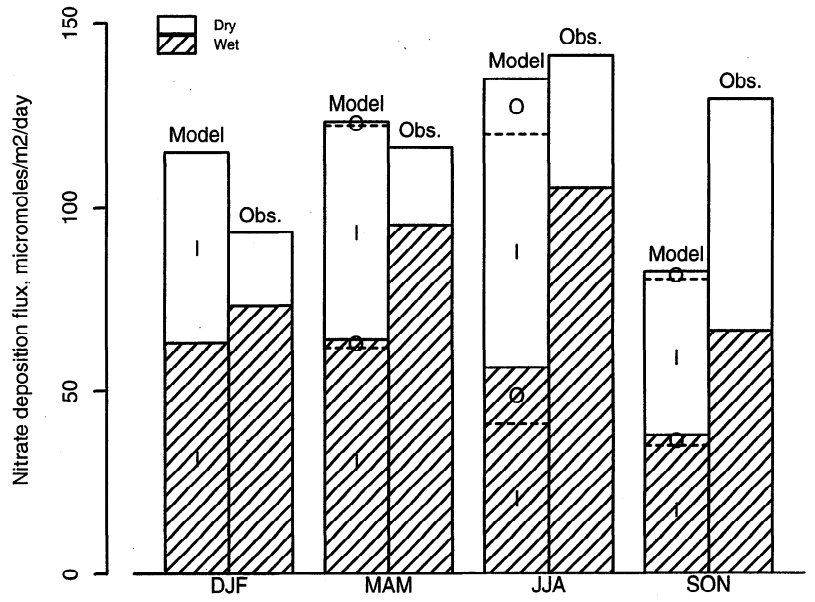

Figure 9. Simulated and observed wet and dry deposition fluxes of NO_3^- at Harvard Forest, Massachusetts in different seasons. Model results are shown separately for NO_3^- produced by inorganic (I) and organic (O) pathways, as described in the text and in Table 3. Reference for the observations is given in Table 2.

Table 3. Budget of fossil fuel combustion NO_y in the U.S. boundary layer

Season	Summer (JJA)	Fall (SON)	Winter (DJF)	Spring (MAM)
Concentration, ppbv				
NO_x	0.21	0.51	0.80	0.36
PAN	0.13	0.11	0.08	0.20
PMN	0.012	0.006	0.003	0.007
PPN (lumped)	0.023	0.020	0.003	0.024
Isoprene nitrates	0.028	0.020	0.001	0.005
Alkylnitrates	0.015	0.015	0.015	0.031
HNO_3	0.55	0.60	0.35	0.29
Total NO_y	1.0	1.3	1.3	0.9
Lifetime, days				
NO_x	0.27	0.64	1.2	0.47
PAN	0.086	0.23	0.95	0.47
HNO_3	0.93	1.1	0.67	0.50
NO_x emission, Gmol d^{-1}	1.34	1.34	1.34	1.34
Dry deposition, Gmol d^{-1}				
NO_x	0.077	0.094	0.064	0.092
PANs	0.030	0.015	0.0039	0.020
RNO_3	0.034	0.023	0.0022	0.010
HNO_3(I)	0.35	0.39	0.39	0.41
HNO_3(O)	0.12	0.051	0.0099	0.037
Total dry deposition	0.62	0.57	0.47	0.57
Wet deposition, Gmol d^{-1}				
HNO_3(I)	0.23	0.30	0.39	0.37
HNO_3(O)	0.14	0.048	0.016	0.052
Total wet deposition	0.37	0.35	0.41	0.42
Export, Gmol d^{-1}				
NO_x	0.10	0.14	0.27	0.15
PANs	0.122	0.108	0.054	0.12
RNO_3	0.027	0.022	0.0090	0.019
HNO_3(I)	0.073	0.13	0.11	0.061
HNO_3(O)	0.026	0.016	0.0021	0.0036
Total export	0.35	0.42	0.46	0.35

All quantities are 3-month averages for the U.S. boundary layer extending horizontally over the area delineated by thick lines in Figure 1 and vertically to the top of model layer 3 (about 740 hPa). The budgets are for NO_y emitted by fossil fuel combustion within the region, as determined by subtracting the background NO_y concentrations and fluxes from the zero-NO_x simulation. PANs includes PAN, PMN, and PPN; RNO_3 includes isoprene nitrates and alkylnitrates. HNO_3(I) denotes HNO_3 of inorganic origin, namely, formed from oxidation of NO_2 by OH and hydrolysis of N_2O_5 in aerosols; HNO_3(O) denotes HNO_3 produced by decomposition of hydroxy organic nitrates (mainly isoprene nitrates). Aerosol nitrate is lumped with HNO_3 in the model. Lifetimes are defined as the concentrations divided by the sum of chemical and deposition loss rates. JJA, June, July, and August; SON, September, October, and November; DJF, December, January, and February; MAN, March, April, and May.

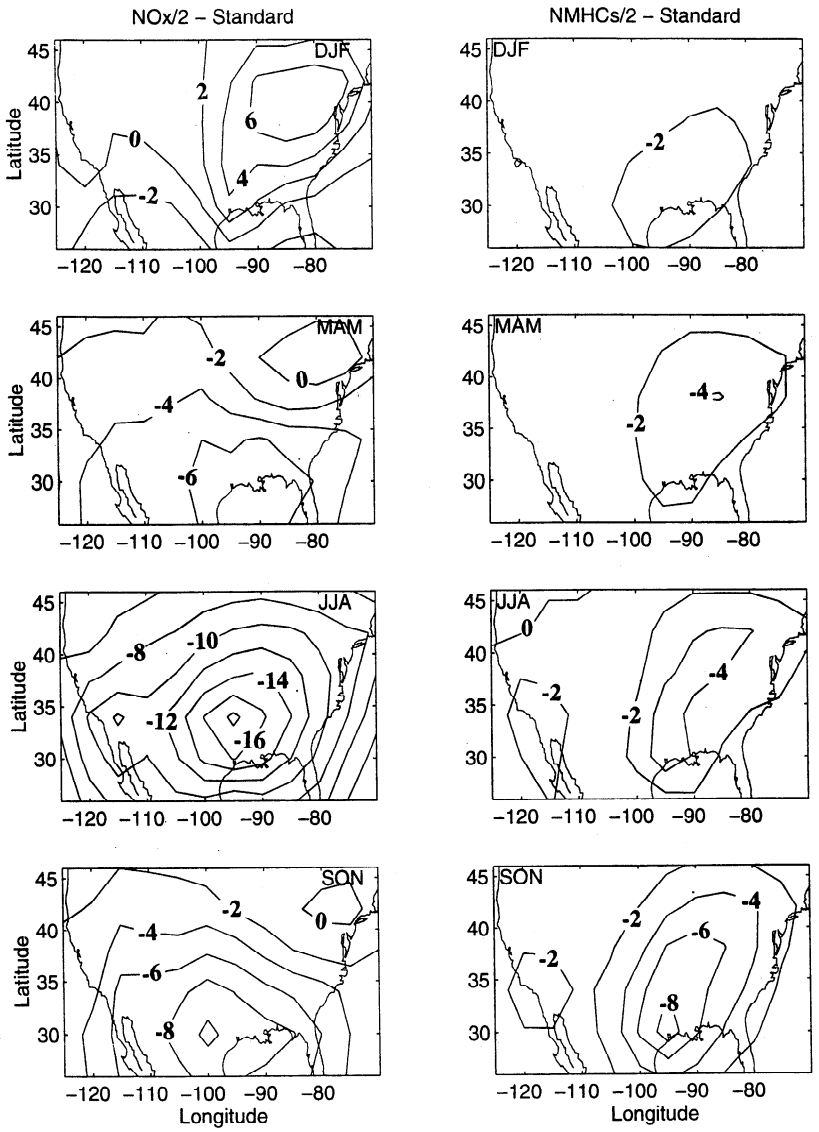

Figure 10. Simulated changes in seasonal mean afternoon O_3 concentrations (ppbv) in surface air resulting from halved emissions of NO_x (left panels) or NMHCs (right panels). The reduction of NMHC emissions is applied to both anthropogenic and biogenic sources.

ranges from 1 Gmol d^{-1} in winter to 6.5 Gmol d^{-1} in summer, for an annual average of 3.8 Gmol d^{-1}.

We thus find that export of U.S. pollution supplies 12 Gmol d^{-1} of O_3 annually to the global troposphere (4 Gmol d^{-1} from direct export of O_3, 8 Gmol d^{-1} from export of NO_x + PANs). Using an earlier version of the model, *Jacob et al.* [1993b] estimated a global source of O_3 from export of U.S. pollution in summer of 8 Gmol d^{-1} (4 Gmol d^{-1} from direct export of O_3, 4 Gmol d^{-1} from export of NO_x, none from export of PANs). In our model the corresponding O_3 source for summer is 17 Gmol d^{-1} (6 Gmol d^{-1} from direct export of O_3, 11 Gmol d^{-1} from export of NO_x + PANs). There were significant problems in the representation of NO_y chemistry in the *Jacob et al.* [1993b] model, including notably the simulation of PANs, which have been corrected in the present version [*Horowitz et al.*, this issue].

The global O_3 source contributed by U.S. pollution can be estimated from our model on an annual basis by adding the 8 Gmol d^{-1} produced within the U.S. boundary layer (Table 4) to the 8 Gmol d^{-1} produced following export of NO_x + PANs, for a total of 16 Gmol d^{-1} (or 5.9 Tmol yr^{-1}). In comparison, a global three-dimensional model study by Y. Wang et al. (Global simulation of tropospheric O_3-NO_x-hydrocarbon chemistry, 2, Model evaluation and global ozone budget, submitted to *Journal of Geophysical Research*, 1997b) (hereinafter referred to as Wang et al., submitted manuscript, 1997b) estimates an annual mean odd oxygen source of 59 Tmol yr^{-1} in the northern hemisphere troposphere and 19 Tmol yr^{-1} for middle and high northern latitudes (30°-90°N). Low latitudes dominate the hemispheric O_3 budget because of the large OPEs. Our results suggest that U.S. pollution makes only a small contribution to O_3 on the scale of the northern hemisphere troposphere but is important on the scale of the extratropical latitudes.

7. Conclusions

We have used a continental-scale, three-dimensional photochemical model to investigate the budgets of NO_y species and O_3 in the continental boundary layer over the United States and to

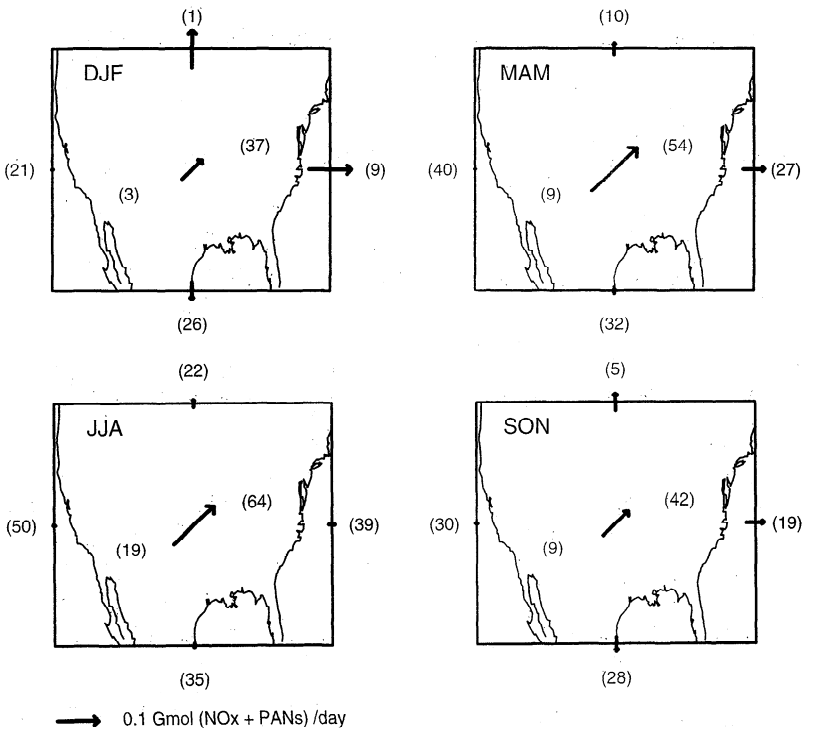

Figure 11. Export of NO_x + PANs from the U.S. boundary layer and related O_3 production efficiency (OPE). The arrows show the seasonal mean export fluxes of NO_x + PANs from the U.S. boundary layer to the west, east, south, north, and free troposphere (above 740 hPa) in the model. The central arrow denotes the upward flux to the free troposphere. The lengths of the arrows are proportional to the fluxes. The numbers in parentheses are the modeled OPEs (mol/mol) in the U.S. boundary layer (lower left of the central arrows), the four adjacent boundary layer regions (margins of the plots), and the free troposphere (upper right of the central arrows). The definition of OPE is given in the text.

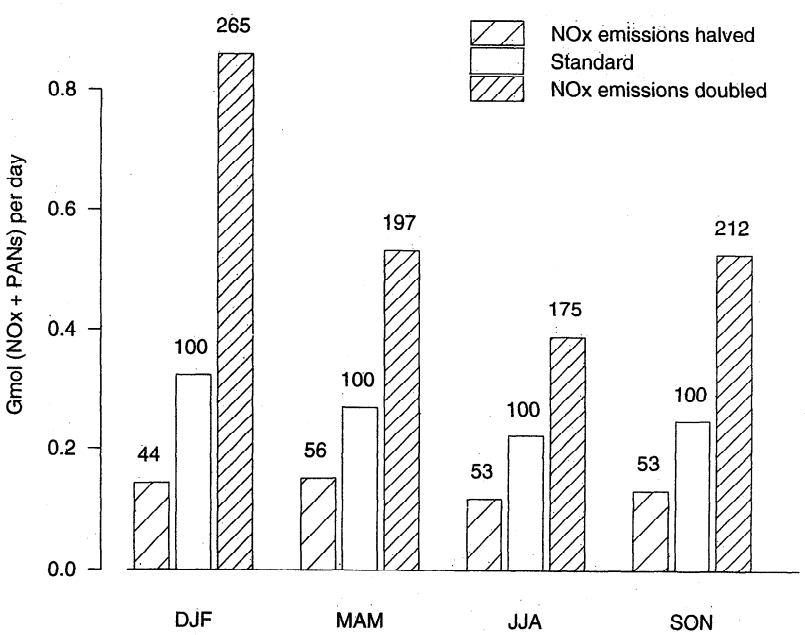

Figure 12. Seasonal mean export fluxes of (NO_x + PANs) from the U.S. boundary layer in the standard simulation and in simulations with halved or doubled NO_x emissions. The percentage changes in the export fluxes for each season, relative to the standard simulation (100%), are shown on top of the bars.

Table 4. Seasonal budgets of ozone in the U.S. boundary layer in the model

Season	Summer(JJA), Gmol d^{-1}	Fall(SON), Gmol d^{-1}	Winter(DJF), Gmol d^{-1}	Spring(MAM), Gmol d^{-1}	Annual, Gmol d^{-1}
		Standard Simulation			
P_{O_x}	15	8.5	3.1	8.3	8.8
L_{O_x}	8.7	4.6	2.5	4.8	5.2
O_3 deposition	4.7	2.9	1.4	3.4	3.0
O_3 export	1.8	1.0	-1.0	-0.50	0.33
P_{O_x} from exported NO_x and PANs[a]	11	5.9	4.8	11	8.2
		Pollution Ozone[b]			
P_{O_x}	13	7.5	2.9	7.9	7.9
L_{O_x}	4.2	2.7	1.7	2.4	2.7
O_3 deposition	2.5	1.2	0.075	1.1	1.2
O_3 export	6.5	3.9	1.0	3.9	3.8

The budgets are given for odd oxygen, O_x (Table 1), to account for the rapid interconversion between O_x species. Since O_3 is the main component of O_x, the budgets of O_3 and O_x can be regarded as equivalent. P_{O_x} and L_{O_x} denote chemical production and destruction of O_x within the U.S. boundary layer.

[a] Estimated O_x production in the remote troposphere contributed by NO_x and PANs molecules exported from the U.S. boundary layer (see text).

[b] Ozone produced in the U.S. boundary layer from anthropogenic NO_x emitted within the region; its budget is obtained by subtracting the O_3 budget in the zero-NO_x simulation from the O_3 budget in the standard simulation.

estimate the exports of these species to the global atmosphere in different seasons. The model indicates a large seasonal variation of the NO_x/NO_y ratio in the U.S. boundary layer, with values ranging from 0.2 in summer to 0.6 in winter; this result is consistent with observations at Harvard Forest, Massachusetts. The seasonal variation of the NO_x/NO_y ratio is driven principally by the seasonal variation of the NO_x chemical lifetime. Formation of hydroxy organic nitrates from the oxidation of isoprene, followed by decomposition of these organic nitrates to HNO_3, accounts for 30% of the NO_x sink in summer in our model. Recent laboratory measurements by P.B. Shepson (personal communication, 1997) indicate a 4.4% yield of hydroxy organic nitrates from oxidation of isoprene, lower than the 12% yield used here [*Tuazon and Atkinson*, 1990; *Paulson and Seinfeld*, 1992; *Atkinson*, 1994] and implying a smaller role of these nitrates in the summertime budget of NO_y. The fraction of NO_y present as PANs in the U.S. boundary layer in the model is highest in spring (25% of total NO_y), reflecting a combination of active photochemistry and low temperatures. Year-round observations of NO_y speciation (including PANs) at U.S. sites would be extremely valuable for testing our understanding of the seasonal variation in the NO_y budget.

We find in the model that 25-35% of NO_x emitted in the United States is exported as NO_y out of the continental boundary layer depending on season and that 60-80% of this export is in the form of NO_x or PANs and hence available to lead to O_3 production in the remote troposphere. The fraction of NO_y present as NO_x or PANs in the exported air is larger than one would expect based on the speciation of concentrations in the U.S. boundary layer, because much of the export (especially in summer) takes place in wet convective updrafts where HNO_3 is efficiently scavenged.

The response of NO_y export to change in NO_x emissions in the United States is found to be less than proportional in summer and more than proportional in winter, reflecting a seasonal transition in the photochemical regime of the continental boundary layer. Doubling NO_x emissions would increase the total export of NO_x and PANs by only 75% in summer but by 165% in winter.

The export of fossil fuel combustion NO_x and PANs from the U.S. boundary layer is estimated to be 1.4 Tg N yr^{-1}. This export represents an important source of NO_x to the northern hemisphere troposphere, comparable to the source from lightning. On the basis of model-derived O_3 production efficiencies for the remote troposphere, we estimate that the NO_x and PANs exported from the United States eventually yield 8 Gmol d^{-1} of O_3 on a global scale. In comparison, direct export of O_3 pollution from the U.S. boundary layer in the model amounts to 4 Gmol d^{-1}. We conclude that the effect of U.S. pollution on global tropospheric O_3 is determined principally, and in all seasons, by the export of NO_x and PANs from the continental boundary layer.

Acknowledgements. This work was supported by the National Oceanic and Atmospheric Administration (NA46GP0138), the National Science Foundation (NSF-ATM-96-12282), and the National Aeronautics and Space Administration (NASA-NAGW-2632 and NASA-NAG5-2688).

References

Atkinson, R., Gas-phase tropospheric chemistry of organic compounds: A review, *J. Phys. Chem. Ref. Data, Monogr., 2,* 1-216, 1994.

Atkinson, R., D.L. Baulch, R.A. Cox, R.F. Hampson, J.A. Kerr, and J. Troe, Evaluated kinetic and photochemical data for atmospheric chemistry, IV, IUPAC subcommittee on gas kinetic data evaluation for atmospheric chemistry, *Atmos. Environ., Part A, 26,* 1187-1230, 1992.

Balkanski, Y.J., D.J. Jacob, G.M. Gardner, W.C. Graustein, and K.K. Turekian, Transport and residence times of tropospheric aerosols inferred from a global three-dimensional simulation of ^{210}Pb, *J. Geophys. Res. 98,* 20,573-20,586, 1993.

Baughcum, S.L., T.G. Tritz, S.C. Henderson, and D.C. Pickett, Scheduled civil aircraft emission inventories for 1992: Database development and analysis, Rep. *NASA CR-4700,* NASA, Washington, D. C., 1996.

Benkovitz, C.M., M.T. Schultz, J. Pacyna, L. Tarrason, J. Dignon, E.C. Voldner, P.A. Spiro, J.A. Logan, and T.E. Graedel,

Global gridded inventories for anthropogenic emissions of sulfur and nitrogen, *J. Geophys. Res., 101*, 29,239-29,253, 1996.

Chameides, W.L., F. Fehsenfeld, M.O. Rodgers, C. Cardetino, J. Martinez, D. Parrish, W. Lonneman, D.R. Lawson, R.A. Rasmussen, P. Zimmerman, J. Greenberg, P. Middleton, and T. Wang, Ozone precursor relationships in the ambient atmosphere, *J. Geophys., Res. 97*, 6037-6055, 1992.

Chin, M., D.J. Jacob, G.M. Gardner, M.S. Foreman-Fowler, P.A. Spiro, and D.L. Savoie, A global three-dimensional model of tropospheric sulfate, *J. Geophys. Res., 101*, 18,667-18,690, 1996.

Crutzen, P.J., The role of NO and NO_2 in the chemistry of the troposphere and stratosphere, *Ann. Rev. Earth Planet. Sci., 7*, 443-472, 1979.

DeMore, W.B., S.P. Sander, D.M. Golden, R.F. Hampson, M.J. Kurylo, C.J. Howard, A.R. Ravishankara, C.E. Kolb, and M.J. Molina, Chemical kinetics and photochemical data for use in stratospheric modeling, Evaluation No. 11, *JPL Publ., 94–1*, Jet Propul. Lab., Pasadena, Calif., 1994.

Dentener, F.J., and P.J. Crutzen, Reaction of N_2O_5 on tropospheric aerosols: impact on the global distribution of NO_x, O_3, and OH, *J. Geophys. Res., 98*, 7149-7163, 1993.

Doddridge, B.G., R.R. Dickerson, R.G. Wardell, K.L. Civerolo, and L.J. Nunnermacker, Trace gas concentrations and meteorology in rural Virginia, 2, Reactive nitrogen compounds, *J. Geophys. Res., 97*, 20,631-20,646, 1992.

Environment Canada, Estimation of the effects of various municipal waste management strategies on greenhouse gas emissions, summary report, Ottawa, Ontario, Canada, 1995.

Fiore, A.M., D.J. Jacob, J.A. Logan, and J.H. Yin, Trends in ground level ozone over the contiguous United States from 1980 to 1995, in press, 1997.

Galloway, J.N., D.M. Whelpdale, and G.T. Wolff, The flux of S and N eastward from North America, *Atmos. Environ., 12*, 2595-2607, 1984.

Goldstein, A.H., S.-M. Fan, M.L. Goulden, J.W. Munger, and S.C. Wofsy, Emissions of ethene, propene, and 1-butene by a midlatitude forest, *J. Geophys. Res., 101*, 9149-9157, 1996.

Gregory, G.L., and A.D. Scott, Compendium of NASA data base for the Global Tropospheric Experiment's Pacific Exploratory Mission-West A (PEM-West A), Rep. *NASA TM-109177*, NASA, Hampton, Va., 1995a.

Gregory, G.L., and A.D. Scott, Compendium of NASA data base for the global tropospheric experiment's Pacific Exploratory Mission-West B (PEM-West B), Rep. *NASA TM-110193*, NASA, Hampton, Va., 1995b.

Grosjean, D., E. Grosjean, and E.L. Williams, Thermal decomposition of PAN, PPN, and vinyl-PAN, *J. Air & Waste Manage. Assoc., 44*, 391-396, 1994.

Guenther, A., C.N. Hewitt, D. Erickson, R. Fall, C. Geron, T. Graedel, P. Harley, L. Klinger, M. Lerdau, W.A. Mckay, T. Pierce, B. Scholes, R. Steinbrecher, R. Tallamraju, J. Taylor, and P. Zimmermann, A global model of natural volatile organic compound emissions, *J. Geophys. Res., 100*, 8873-8892, 1995.

Hansen, J., G. Russell, D. Rind, P. Stone, A. Lacis, S. Lebedeff, R. Ruedy, and L. Travis, Efficient three-dimensional global models for climate studies: Models I and II, *Mon. Weather Rev., 111*, 609-662, 1983.

Holzworth, G.C., Mixing depths, wind speeds and air pollution potentials for selected locations in the United States, *J. Appl. Meteorol., 6*, 1039-1044, 1967.

Horowitz, L.W., J. Liang, G.M. Gardner, and D.J. Jacob, Export of reactive nitrogen from North America during summertime: Sensitivity to hydrocarbon chemistry, *J. Geophys. Res.*, this issue.

Intergovernmental Panel on Climate Change (IPCC), *Climate Change 1994*, edited by J.T. Houghton et al., p. 99, Cambridge Univ. Press, New York, 1995.

Jacob, D.J., and M.J. Prather, Radon-222 as a test of convective transport in a general circulation model, *Tellus, Ser. B*, 118-134, 1990.

Jacob, D.J., et al., Simulation of summertime ozone over North America, *J. Geophys. Res., 98*, 14,797-14,816, 1993a.

Jacob, D.J., J.A. Logan, G.M. Gardner, R.M. Yevich, C.M. Spivakovsky, S.C. Wofsy, S. Sillman, and M.J. Prather, Factors regulating ozone over the United States and its export to the global atmosphere, *J. Geophys. Res., 98*, 14,817-14,826, 1993b.

Jacob, D.J., L.W. Horowitz, J.W. Munger, B.G. Heikes, R.R. Dickerson, R.S. Artz, and W.C. Keene, Seasonal transition from NO_x- to hydrocarbon-limited ozone production over the eastern United States in September, *J. Geophys. Res., 100*, 9315-9324, 1995.

Jacob, D.J., and 29 others, Evaluation and intercomparison of global atmospheric transport models using ^{222}Rn and other short-lived tracers, *J. Geophys. Res., 102*, 5953-5970, 1997.

Jacobson, M.Z., and R.P. Turco, SMVGEAR: a sparse-matrix, vectorized Gear code for atmospheric models, *Atmos. Environ., Part A, 28*, 273-284, 1994.

Kasibhatla, P.S., H. Levy II, and W.J. Moxim, Global NO_x, HNO_3, PAN, and NO_y distributions from fossil fuel combustion emissions: A model study, *J. Geophys. Res., 98*, 7165-7180, 1993.

Kirchner, F., and W.R. Stockwell, Effect of peroxy radical reactions on the predicted concentrations of ozone, nitrogenous compounds, and radicals, *J. Geophys. Res., 101*, 21,007-21,022, 1996.

Liang, J., and D.J. Jacob, Effect of aqueous-phase cloud chemistry on tropospheric ozone, *J. Geophys. Res., 102*, 5993-6001, 1997.

Liu, S.C., M. Trainer, F.C. Fehsenfeld, D.D. Parrish, E.J. Williams, D.W. Fahey, G. Hubler, and P.C. Murphy, Ozone production in the rural troposphere and the implications for regional and global ozone distributions, *J. Geophys. Res., 92*, 4191-4207, 1987.

Logan, J.A., Nitrogen oxides in the troposphere: Global and regional budgets, *J. Geophys. Res., 88*, 10,785-10,807, 1983.

Logan, J.A., Ozone in rural areas of the United States, *J. Geophys. Res., 94*, 8511-8532, 1989.

Logan, J.A., M.J. Prather, S.C. Wofsy, and M.B. McElroy, Tropospheric chemistry, A global perspective, *J. Geophys. Res., 86*, 7210-7254, 1981.

Maricq, M. M., and J. J. Szente, Kinetics of the reaction between ethylperoxy radical and nitrogen oxide, *J. Phys. Chem., 100*, 12,374-12,379, 1996a.

Maricq, M. M., and J. J. Szente, Temperature-dependent study of the reaction between peroxyacetyl radicals and nitrogen oxide, *J. Phys. Chem., 100*, 12,380-12,385, 1996b.

McKeen, S.A., E.-Y. Hsie, and S.C. Liu, A study of the dependence of rural ozone on ozone precursors in the eastern United States, *J. Geophys. Res., 96*, 15,377-15,394, 1991.

Monson, R.K., P.C. Harley, M.E. Litrak, M. Wildermuth, A.B. Guenther, and P.R. Zimmermann, Environmental and development controls over the seasonal pattern of isoprene emission from aspen leaves, *Oecologia, 99*, 260-270, 1994.

Mozurkewich, M., and J. G. Calvert, Reaction probability of N_2O_5 on aqueous aerosols, *J. Geophys. Res., 93*, 15,889-15,896, 1988.

Olson, J., World ecosystems (WE1.4): Digital raster data on a 10 minute geographic 1080 x 2160 grid, in *Global Ecosystems Database, Version 1.0: Disc A*, edited by NOAA Nat. Geophys. Data Cent., Boulder, Colo., 1992.

Oltmans, S.J., and H. Levy II, Seasonal cycles of surface ozone over the western North Atlantic, *Nature, 358*, 392-394, 1992.

Paulson, S.E., and J.H. Seinfeld, Development and evaluation of a photooxidation mechanism for isoprene, *J. Geophys. Res., 97,* 20,703-20,715, 1992.

Perros, P.E., Large-scale distribution of peroxyacetylnitrate from aircraft measurements during the TROPOZ II experiment, *J. Geophys. Res., 99,* 8269-8279, 1994.

Poulida, O., R.R. Dickerson, B.G. Doddridge, J.Z. Holland, R.G. Wardell, and J.G. Watkins, Trace gas concentrations and meteorology in rural Virginia, 1, Ozone and carbon monoxide, *J. Geophys. Res., 96,* 22,461-22,475, 1991.

Prather, M.J., M.B. McElroy, S.C. Wofsy, G. Russell, and D. Rind, Chemistry of the the global troposphere: Fluorocarbons as tracers of air motion, *J. Geophys. Res., 92,* 6579-6613, 1987.

Shepson, P.B., E. Mackay, and K. Muthuramu, Henry's Law constants and removal processes for several atmospheric β-hydroxy alkyl nitrates, *Environ. Sci. Technol., 30,* 3618-3623, 1996.

Sillman, S., J.A. Logan, and S.C. Wofsy, A regional scale model for ozone in the United States with subgrid representation of urban and power plant plumes, *J. Geophys. Res., 95,* 5731-5748, 1990a.

Sillman, S., J.A. Logan, and S.C. Wofsy, The sensitivity of ozone to nitrogen oxides and hydrocarbons in regional ozone episodes, *J. Geophys. Res., 95,* 1837-1851, 1990b.

Singh, H.B., Reactive nitrogen in the troposphere, *Environ. Sci. Technol., 21,* 320-327, 1987.

Singh, H.B., et al., Latitudinal distribution of reactive nitrogen in the free troposphere over the Pacific Ocean in late winter/early spring, *J. Geophys. Res.*, in press, 1997.

Sirois, A., and J.W. Bottenheim, Use of backward trajectories to interpret the 5-year record of PAN and O_3 ambient air concentrations at Kejimkujik National Park, Nova Scotia, *J. Geophy. Res., 100,* 2867-2881, 1995.

Spivakovsky, C.M., R. Yevich, J.A. Logan, S.C. Wofsy, M.B. McElroy, and M.J. Prather, Tropospheric OH in a three-dimensional chemical tracer model: An assessment based on observations of CH_3CCl_3, *J. Geophys. Res., 95,* 18,441-18,472, 1990.

Thompson, A.M., K.E. Pickering, R.R. Dickerson, W.G. Ellis, D.J. Jacob, J.R. Scala, W.-K. Tao, D.P. McNamara, and J. Simpson, Convective transport over the central United States and its role in the regional CO and ozone budgets, *J. Geophys. Res., 99,* 18,703-18,711, 1994.

Trainer, M., E.J. Williams, D.D. Parrish, M.P. Buhr, E.J. Allwine, H.H. Westberg, F.C. Fehsenfeld, and S.C. Liu, Models and observations of the impact of natural hydrocarbons on rural ozone, *Nature, 329,* 705-707, 1987.

Tuazon, E.C., and R. Atkinson, A product study of the gas-phase reaction of isoprene with the OH radical in the presence of NO_x, *Int. J. Chem. Kinet., 22,* 1221-1236, 1990.

U.S. Environmental Protection Agency (U.S. EPA), The 1985 NAPAP emission inventory (version 2): Development of the annual data and modeler's tapes, Rep. *EPA-600/7-89-012a,* Research Triangle Park, N. C., 1989.

U.S. EPA, National air pollutant emissions estimates, 1900-1994, Rep. *EPA-454/R-95-011,* Research Triangle Park, N. C., 1995.

U.S. National Acid Precipitation Assessment Program (NAPAP), 1990 integrated assessment report, Off. of the Dir., Washington, D. C., 1991.

Wesely, M.L., Parameterization of surface resistance to gaseous dry deposition in regional-scale numerical models, *Atmos. Environ., 23,* 1292-1304, 1989.

A. M. Fiore, G. M. Gardner, L.W. Horowitz, D. J. Jacob (corresponding author), J. A. Logan, J. W. Munger, and Y. Wang, Department of Earth and Planetary Sciences, Harvard University, Cambridge, MA 02138. (e-mail: djj@io.harvard.edu)

J. Liang, Department of Civil and Environmental Engineering, Stanford University, Stanford, CA 94041. (e-mail: jliang@standord.edu)

(Received March 26, 1997; revised October 21, 1997; accepted October 29, 1997.)